

Using Model-Scale Tandem-Rotor Measurements in Ground Effect to Understand Full-Scale CH-47D Outwash



Manikandan Ramasamy*

*U.S. Army Aviation Development Directorate —AFDD
Aviation & Missile Research, Development & Engineering Center
Research, Development & Engineering Command
Ames Research Center, Moffett Field, CA*



Gloria K. Yamauchi
*Aeromechanics Office
NASA Ames Research Center
Moffett Field, CA*

Downwash and outwash characteristics of a model-scale tandem-rotor system in the presence of the ground were analyzed by identifying and understanding the physical mechanisms contributing to the observed flow field behavior. A building block approach was followed in simplifying the problem, separating the effects of the fuselage, effects of one rotor on the other, etc. Flow field velocities were acquired in a vertical plane at four aircraft azimuths of a small-scale tandem rotor system using the particle image velocimetry technique for radial distances up to four times the rotor diameter. Results were compared against full-scale CH-47D measurements. Excellent correlation was found between the small- and full-scale mean flow fields (after appropriate normalization using rotor and wall jet parameters). Following the scalability analysis, the effect of rotor height on the outwash was also studied. Close to the aircraft, an increase in rotor height above ground decreased the outwash velocity at all aircraft azimuths. However, farther away, the longitudinal and lateral axes of the aircraft showed increasing and decreasing outwash velocities, respectively, with increasing rotor height. Baseline rotor measurements were made out-of-ground effect to understand the nature of inflow distribution for realistic rotor configurations and their modified characteristics in the presence of the ground.

Nomenclature

C_T	thrust coefficient
D	diameter of the rotor
h	rotor height above ground
r	radial distance from the aircraft reference center
V_h	hover-induced velocity using momentum theory
V_r	component of velocity along the r -coordinate
V_z	component of velocity along the z -coordinate
z	normal distance from the ground ($z = 0$ at ground)
z_r	normal distance from the rotor plane ($z_r = 0$ at rotor plane)
$z_{1/2}$	wall jet half-height

Introduction

Assessment of the operational impact of rotorwash (downwash + outwash) is becoming increasingly necessary when designing next-generation aircraft. Designers are often required to identify strategies to

mitigate the detrimental effects of rotorwash (Refs. 1, 2) on both ground personnel and surrounding facilities. Mitigating rotorwash requires developing a comprehensive knowledge of a large number of rotor parameters that affect the flow field characteristics of rotors. In the case of single rotors, these parameters include but are not limited to helicopter gross weight, rotor radius, rotor height above the ground, disk loading, and loading distribution. In the case of multirotor configurations, the number of rotors, distance between the rotors, and the presence or absence of rotor overlap also play a substantial role in dictating the outwash velocity magnitudes. Furthermore, the location of a person or object with respect to the aircraft becomes a variable for tilt- and tandem-rotor configurations because the flow field is asymmetric about the aircraft center unlike the symmetric rotorwash field of single- and coaxial-rotor configurations.

The U.S. Army Conceptual Design & Assessment Office currently uses a first-order momentum-based model (RoWFoot (Ref. 2)) to estimate the effects of rotor parameters on rotorwash. Momentum-based models are ideal for design analysis as they are computationally fast—a necessary trait considering the number of parameters that affect rotorwash velocities. A detailed history on the development of such models is given in Ref. 3. RoWFoot is semiempirical and requires data for not only deriving empirical constants but also to validate the resulting predictions. As with any semiempirical model, the confidence in RoWFoot predictions reduces significantly when applied beyond the operating conditions and configurations of the experiments from where the empirical constants were derived.

*Corresponding author; e-mail: manikandan.ramasamy.civ@mail.mil.
Presented in part at the American Helicopter Society 71st Annual Forum, Virginia Beach, VA, May 5–7, 2015. Manuscript received August 2015; accepted June 2016.

Table 1. Past experiments on a rotor operating IGE

Reference	Type (Aircraft)	Scale/Diameter
Taylor (1950) (Ref. 4)	S, C, Ta	20 and 45 inches
Fradenburgh (1958) (Ref. 5)	S	24 inches
Bolanovich and Marks (1959) (Ref. 6)	S	75 ft
Bryan (1960) (Ref. 7)	Ti(VZ-2)	28 inches and 9 ft
Newsom and Tosti (1962) (Ref. 8)	Ti(VZ-2, X-18)	1/4–1/8 scale
Michaelsen (1971) (Ref. 9)	S (S-61) & Ti (CL-84)	Full scale
Harris (1976) (Ref. 10)	S(CH-53E)	Full scale
Velkoff (1985) (Ref. 11)	S	5 and 7.2 ft
Light (1989) (Ref. 12)	S	3.62 ft
Meyerhoff (1990) (Ref. 13)	Ti (MV-22)	Full scale
Lake (1998) (Ref. 14)	Ti(MV-22)	Full scale
Wadcock (2005) (Ref. 15)	V-22	1/40th scale
Wadcock et al. (2008) (Ref. 16)	S(UH-60L)	Full scale
Nathan and Green (2008) (Ref. 17)	S	7 inches
Johnson et al. (2009) (Ref. 18)	S	7 inches
Lee et al. (2010) (Ref. 19)	S	6.7 inches
Wong and Tanner (2010) (Ref. 20)	S(EH60-L)	Full scale
Milluzzo et al. (2010) (Refs. 21,22)	S	32 inches
Sydney and Leishman (2011) (Ref. 23)	S	7 and 32 inches
Silva and Riser (2011) (Ref. 24)	Ta(CH-47D)	Full scale
Glaser and Jones (2012) (Ref. 25)	S	6.7 inches
Present study	Ta(CH-47D)	1/56th scale

Abbreviations: S, single; C, coaxial; Ta, tandem; Ti, tilt.

Data sets to support RoWFoot can come from model- and full-scale experiments or validated higher order mathematical models. A feasibility study on using high-fidelity computational fluid dynamic (CFD) analysis to model an isolated rotor configuration in ground effect (IGE) at full-scale Reynolds number was conducted in Ref. 3. While the results were encouraging, the study demonstrated the practical challenges associated with predicting rotor outwash in terms of computational expense, boundary conditions, turbulence modeling, flow unsteadiness, the large number of rotor revolutions required to stabilize the flow field, etc. These challenges make CFD rotorwash simulations currently not practical, leaving model- or full-scale measurements as the possible alternative.

Table 1 presents the majority of the flow field measurements made on helicopter rotors operating IGE (Refs. 4–25). Despite a long list (available from the early 1950s) of experiments consisting of a range of rotor configurations tested IGE, Ref. 2 still recommends acquiring more data. This recommendation, however, is understandable when the requirements for mathematical model development and validation are compared against the number of available measurements.

Challenges

Table 1 includes a small subset of full-scale measurements, which are generally preferred over model-scale measurements because of Reynolds number issues. However, there are serious limitations in acquiring a comprehensive full-scale data set. First, full-scale experiments are expensive. Consequently, measurements often quantify the effect of only one or two rotor parameters on rotorwash. For example, the effects of gross weight of the helicopter and rotor height above the ground are the two parameters studied by Silva and Riser (Ref. 24). Second, for a given full-scale configuration (i.e., tandem/tilt rotor) changing rotor parameters is not practical. For example, varying rotor-rotor overlap and/or vertical distance is both expensive and time consuming. As a result, the effects of many rotor parameters (listed earlier) on rotorwash are still poorly understood.

Safety and practical limitations prevent comprehensive measurements during full-scale flight experiments. Velocity measurements under the rotor disk ($r/R < 0.8$) bring up safety concerns and any measurement high above ground (> 12 ft) introduces practical challenges in terms of instrumentation. Furthermore, full-scale experiments often use point measurement techniques that result in arrays of sparse point measurements. Such measurements may be useful for validating computational predictions, but may not be sufficient for understanding the physics of the flow. Lastly, full-scale flight experiments suffer from atmospheric fluctuations and pilot control adjustments, influencing the measured velocities. Experiments conducted under a controlled environment are necessary to eliminate ambiguity in understanding flow development. For the aforementioned reasons, cost-effective alternatives such as model-scale experiments conducted under controlled conditions are necessary. The primary challenge in model-scale measurements is the operating low Reynolds number and the associated scalability issues.

Clear direction in conducting scalability studies is lacking in the literature. The choices of characteristic variables (to normalize measured velocities and length scales) that allow model-scale and full-scale comparison are not conclusive. For example, rotor tip speed and hover-induced velocity (based on uniform inflow momentum theory (V_h), and $2 \times V_h$) have been used to normalize downwash and outwash velocities. For a length scale, the rotor radius, rotor diameter, height above ground, and $R/0.707$ have all been used in the past. In the early 1960s, George et al. (Ref. 26) made an assumption that the flow field of a rotor operating IGE is similar to that of an impinging jet. This allowed George et al. to treat rotor outwash as Glauert's wall jet (Ref. 27) and develop first-order momentum-based rotorwash models. Being self-similar, Glauert's solution identified three key parameters. In terms of rotor variables, the three parameters are (1) shape function of the velocity profile normal to the ground, (2) peak mean outwash velocity decay, and (3) half-height growth of the outwash profile.

To enable scalability studies using Glauert's wall jet theory, measurements are needed radially outward of at least $0.75D$ from the rotor shaft axis where flow development exhibits wall jet-like behavior (Ref. 26).

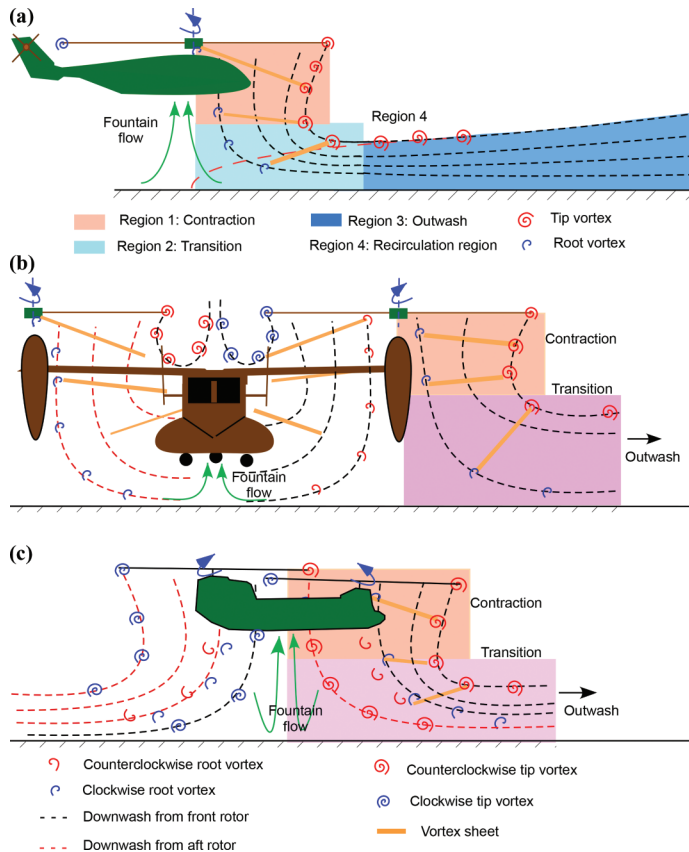


Fig. 1. Flow complexities in tilt and tandem rotors.

While full-scale measurements are available up to $4D$ from the rotor shaft axis, the majority of the model-scale measurements are limited to a small region $0.35 < r/D < 1$, as they were aimed at understanding brownout phenomena. However, following Glauert’s analogy, two studies (Refs. 7, 15) compared model-scale and full-scale measurements with both using tilt rotors along the noninteracting port side of the system in the region $1.5 > r/D > 5$. Bryan’s results (Ref. 7) showed that the peak mean outwash velocity decay is not scalable, i.e., measured peak mean outwash velocity decay on model-scale Vertol VZ-2 (single rotor) was found to be faster than the full-scale tests. However, Wadcock (Ref. 15) showed that the model-scale measurements correlated well with full-scale tests in terms of peak outwash velocity decay and in the shape of the velocity profile. Wadcock’s results suggest that the results are scalable, which contradicts earlier findings from Bryan (Ref. 7). Neither study, however, evaluated the growth of the wall jet, the third characteristic of rotor outwash in terms of scalability.

No comparison along the interacting plane (where flow from the two rotors interact/merge to form a wall jet) has ever been made between the model- and full-scale rotors. However, they are necessary, especially for tandem rotor configurations because the flow at any given azimuth around the tandem rotor aircraft has contributions from both rotors as a result of overlap. This is true even in front of the forward rotor as seen in Fig. 1(c).

One of the primary goals of the present study is to conduct a comprehensive scalability analysis on tandem rotor configurations by evaluating all three variables suggested by Glauert at four aircraft azimuths that include both longitudinal and lateral planes as shown in Fig. 2. Taking advantage of the existing full-scale CH-47D rotor measurements made by Silva and Riser (Ref. 24), the present study measures and compares model-scale tandem rotor measurements under similar operating condi-

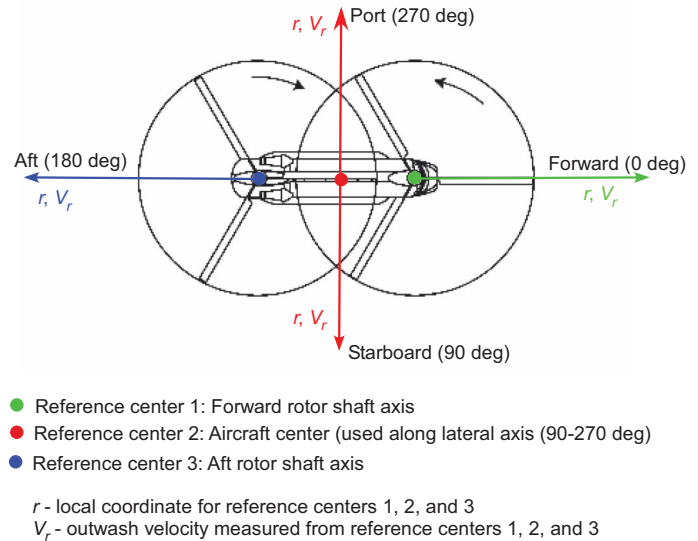


Fig. 2. Coordinate system and reference locations for outwash study.

tions with respect to the full-scale test. The present study also addresses the effect of the fuselage on the rotorwash velocities to evaluate whether past experiments conducted with or without the fuselage may be used to improve understanding of rotorwash.

Finally, very limited downwash data under the rotor disk are available in the literature because of safety concerns during full-scale tests. The majority of model-scale measurements were focused near the tip of the rotor blades and outward to understand brownout. However, understanding the flow under the rotor disk is essential for mathematical model (like RoWFoot) development as the outwash velocities are often estimated from downwash velocities after applying conservation of energy principles (Ref. 2). In the case of tandem rotors, downwash measurements are even more important than for single rotors because of the rotor overlap and the resulting higher downwash along the lateral plane of the aircraft.

In summary, flow field measurements were acquired in a vertical plane out to four rotor diameters. The measurements included the four primary azimuthal positions (forward, aft, starboard, and port). The purpose was to compare the model-scale results with the mean outwash velocities from full-scale measurements made by Silva and Riser (Ref. 24). To understand the influence of one rotor on the other in terms of outwash velocities, a parametric assessment was completed using various (single- and tandem-rotor) configurations. The experimental approach also permitted the effect of the fuselage and rotor height to be assessed and compared against full-scale measurements.

Description of Experiment

Figure 3 shows the set of experiments conducted in the present study. All the experiments were conducted in the U.S. Army hover chamber (25- × 25- × 30-ft high) at NASA Ames Research Center. The large testing volume ensured that flow recirculation effects were minimal.

Model aircraft. Figure 4 shows the model-scale aircraft (1/56th-scale CH-47D; $D = 1.07$ ft; see Ref. 28 for details) used in the present study. Table 2 provides the basic aircraft characteristics for the full-scale CH-47D and model-scale tandem-rotor aircraft. The radio-controlled aircraft model (Fig. 4) was mounted above a two-piece ground plane. To simulate the hover configuration, the front rotor shaft was replaced with a longer shaft so that both rotors were at the same height above the ground plane, similar to the full-scale CH-47D hover configuration (see Fig. 9 of Ref. 24). For the model aircraft, the shaft angles of the forward and aft

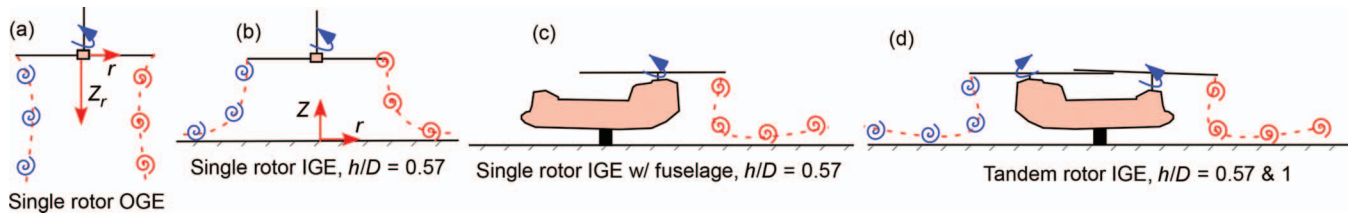


Fig. 3. Configurations tested in this study.

Table 2. Aircraft characteristics

Description	Full scale (Ref. 24)	Model scale
Number of rotors	2	2
Blades per rotor	3	3
Rotor radius (inches)	360	6.31
Rotor-rotor distance (inches)	470	8.33
Solidity	0.0849	0.057
RPM	225	3540
Tip speed (ft/s)	706.9	194.9
Aircraft gross weight or thrust (lb)	41,000	0.96
Disk loading (lb/ft ²)	7.25	0.55
Rotor rotation (fwd/aft)	CCW/CW	CCW/CW
Shaft tilt (deg, + fwd) – fwd/aft	9/4	2.5/0

rotors were 2.5° (forward tilt) and 0°, respectively. Using the simplified hover trim attitude described in Ref. 24, the shaft angles of the full-scale CH-47D were estimated as 2.3° (forward tilt) and 2.5° (aft tilt) for the forward and aft rotors, respectively.

A load cell, shown in Fig. 4, was sandwiched between two plates and mounted in line with each rotor. Coefficient of thrust (C_T) of the model-scale tandem rotor was maintained at approximately 0.0061, which is equivalent to 41,000 lb of full-scale CH-47D rotor thrust. The target C_T for the model-scale tandem rotor was achieved by ensuring equal thrust-sharing between the two rotors (i.e., $C_{T \text{ forward}} = C_{T \text{ aft}} = 0.00305$). For all measurements related to single-rotor configuration (both out of ground effect (OGE) and IGE, with and without fuselage), the rotor thrust was maintained at half the model-scale tandem-rotor system thrust (i.e., $C_T = 0.00305$). This allowed comparative studies to be conducted among various rotor configurations. For example, comparing the flow field of the single rotor and the forward rotor (of the tandem rotor system) that produces the same thrust provides the effect of interaction between the two overlapping rotors. The entire test was conducted at a rotor RPM = 3540 ($V_{tip} = 195 \text{ ft/s}$).

To evaluate flow field differences between the single rotor and two overlapping rotors, the forward rotor was removed while flow measurements were acquired for 180° (aft) aircraft azimuth (Fig. 3(c)). The approximate flow field of an isolated rotor IGE was acquired by removing the front rotor and fuselage, inverting the model above the ground plane, and reversing the direction of thrust. The inversion was necessary to minimize the hardware effects on the rotor flow.

Velocity field measurements IGE were conducted for two rotor heights above the ground (Fig. 3(d); $h/D = 0.578$ and 1.0), matching full-scale test conditions reported in Ref. 24. Also, consistent with the full-scale measurements, the radial span of the measurements extended up to 4 diameters.

PIV system. Figure 5 shows the three 16-MP cameras viewing the laser sheet orthogonally. Each camera viewed a region of interest (ROI) approximately 18 inches wide with an overlap of about 2 inches between camera ROIs. A single calibration target (800 mm high × 1000 mm wide) was used to calibrate all three cameras simultaneously. Particle

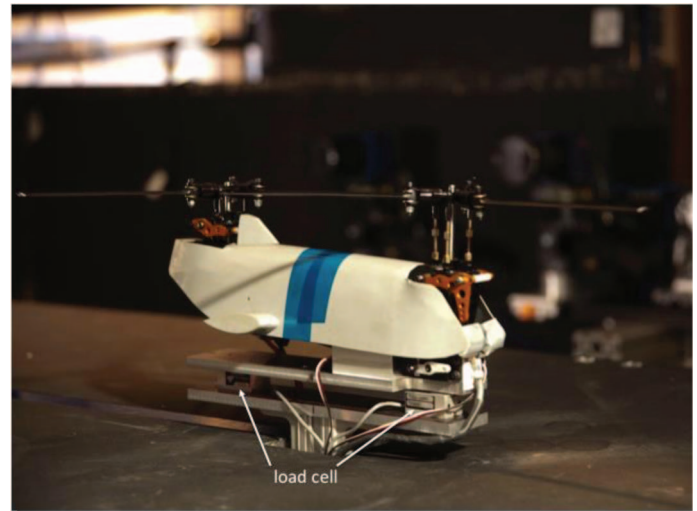


Fig. 4. Model-scale tandem rotor system.

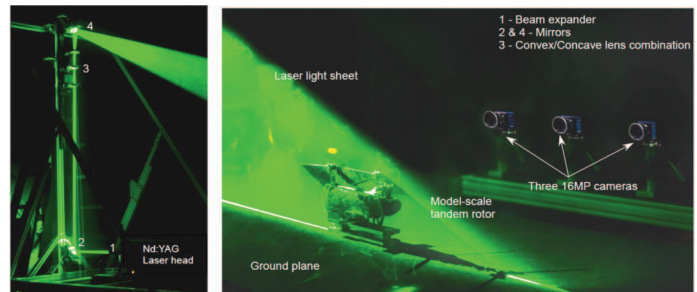


Fig. 5. Experimental setup.

image velocimetry (PIV) images were acquired in two modes: phase locked with the rotor and free run. Only free-run results are shown in this study. For each test condition, 500 image pairs were acquired at 0.49 Hz simultaneously from the three cameras. After processing the images, the instantaneous vector fields were stitched then averaged.

Since the laser sheet and cameras remained stationary, the mount, with model attached, was rotated to acquire flow measurements at four aircraft survey azimuths: 0° (forward of aircraft), 90° (starboard), 180° (aft of aircraft), and 270° (port). The coordinate system and reference centers used in this study follows the convention used in full-scale CH-47D measurements (Ref. 24) and is shown in Fig. 2.

Results

Baseline isolated single-rotor measurements operating in hover OGE will be discussed first. Following this, flow field measurements made IGE will be analyzed. Since limited full-scale data are available for validation, observations made in the past from single/multiple rotors both with and

without a fuselage are compared against the present measurements wherever possible along with the full-scale CH-47D measurements (Ref. 24). Because the present scalability study follows Glauert’s wall jet analogy, model-scale measurements are compared with full-scale measurements only in the outwash region where wall jet-like flow is expected.

Isolated single-rotor OGE

The objective of this measurement was to establish the baseline wake characteristics, specifically the downwash distribution, for a single isolated rotor in hover. The isolated rotor configuration (Fig. 3(a)) was achieved by removing the front rotor blades and fuselage of the tandem rotor model, thereby removing any effect of blade overlap on the inflow distribution. Also, the ground plane was removed and the model rotated so that the rotor axis was horizontal. The wake was therefore unimpeded for more than 15 rotor diameters. Establishing a baseline is necessary because existing rotorwash models use simple momentum theory by assuming that the downwash accelerates to twice the inflow velocity measured at the rotor plane. However, reality is far different

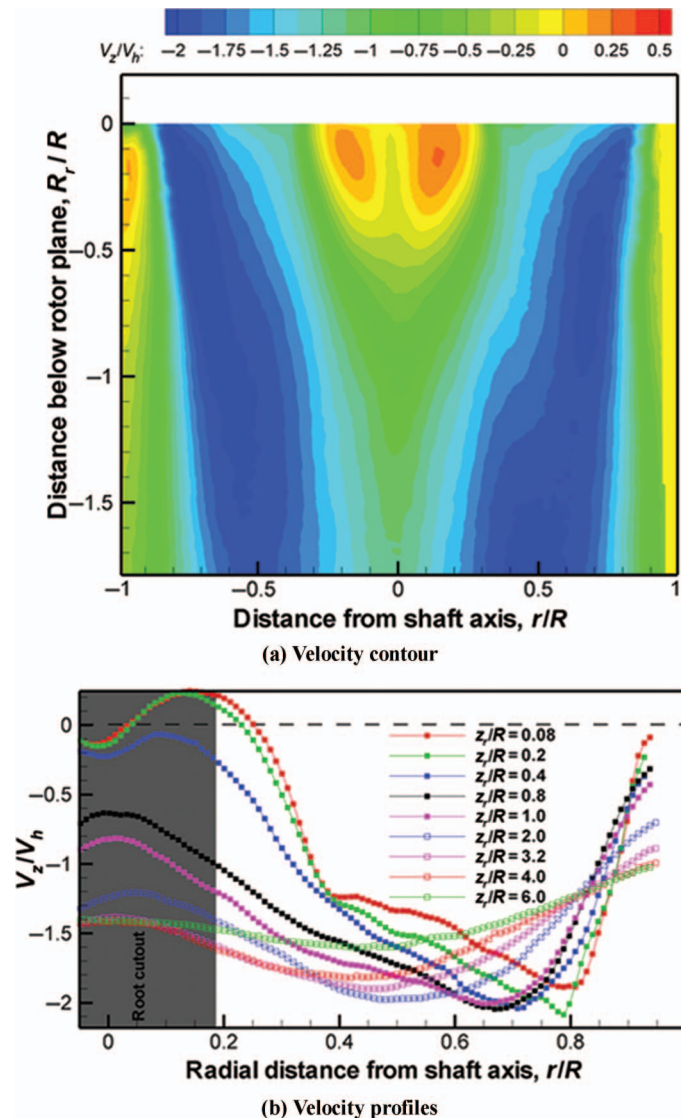


Fig. 6. Vertical component of velocity for the isolated single rotor in hover (OGE).

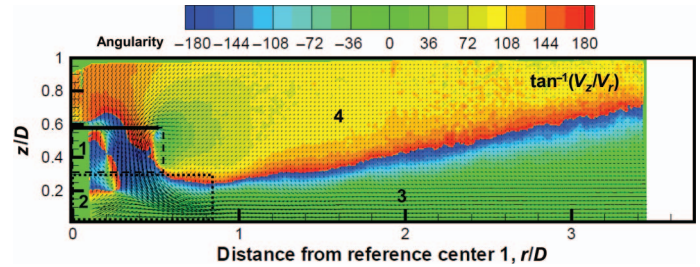


Fig. 7. Time averaged flow field of tandem rotor IGE (forward rotor, $h/D = 0.578$).

from momentum theory assumptions in that the effects of a finite number of blades, tip vortices, and root cut-out play a substantial role in the resulting nonuniform inflow distribution. Accurate representation of the inflow distribution is the first step in downwash prediction.

The vertical component of velocity for the isolated single-rotor configuration is shown in Fig. 6. The velocity data are normalized by the hover-induced velocity from momentum theory $V_h = \sqrt{T/2\rho A}$. Corresponding vertical velocity profiles at various downstream distances are shown in Fig. 6(b). At the center, even though the rotor operated OGE, flow recirculation occurred below the nonlifting portion of the blade, i.e., near the root cut-out. Recirculation was continuously energized by the blade root vortex that transferred momentum from the outboard downwash velocity.

Although the root cut out is only $\approx 18\%$ of the rotor radius, the region of recirculation extends up to $r/R = 0.26$ in the near wake (at about $0.08R$ below the rotor) and gradually reduces with increasing vertical distance before disappearing at about $0.4R$ below the rotor. Nevertheless, the center of rotor flow still had low-momentum flow downstream of the rotor. Consequently, viscous shear continuously transferred momentum from the accelerating downwash velocity to the low-momentum region. The result of the transfer of momentum is evident in the velocity profiles of Fig. 6(b). The velocity deficit near the center of the rotor was found to gradually reduce with increasing z_r/R . At $z_r/R = 6$, downwash velocity is almost uniform across the rotor disk. As Spalart suggested, at even greater downstream distances, the rotor wake may begin behaving like a jet with maximum velocity found near the center rather than at the edges (Ref. 29). Additional analysis on the hovering rotor wake measurements OGE acquired in this test is given in Ref. 3.

In ground effect

Having established the downwash distribution beneath the rotor in hover OGE, the next step is to understand and characterize the rotorwash of a tandem rotor system IGE.

A tandem rotor system with overlapping blades is unique in that the flow characteristics vary around the aircraft azimuth. Any effort to understand the rotorwash of the tandem rotor system should begin with quantifying the influence of one rotor on the other. In this model-scale experiment, the influence was discerned by simply removing the blades from either the forward or the aft rotor. In addition, the fuselage was removable which allowed studies on an isolated rotor IGE to be conducted. Such a building-block approach was essential for understanding the flow mechanisms contributing to the rotorwash behavior of a helicopter with overlapping rotors.

Figure 7 shows the time-averaged flow angularity for the forward rotor of the tandem rotor system IGE over the entire measurement distance. Blue regions indicate mainly vertical flow, whereas green represents mainly horizontal flow. Similar results were obtained for all rotor configurations and azimuths. The angularity parameter in Fig. 7 distinguishes

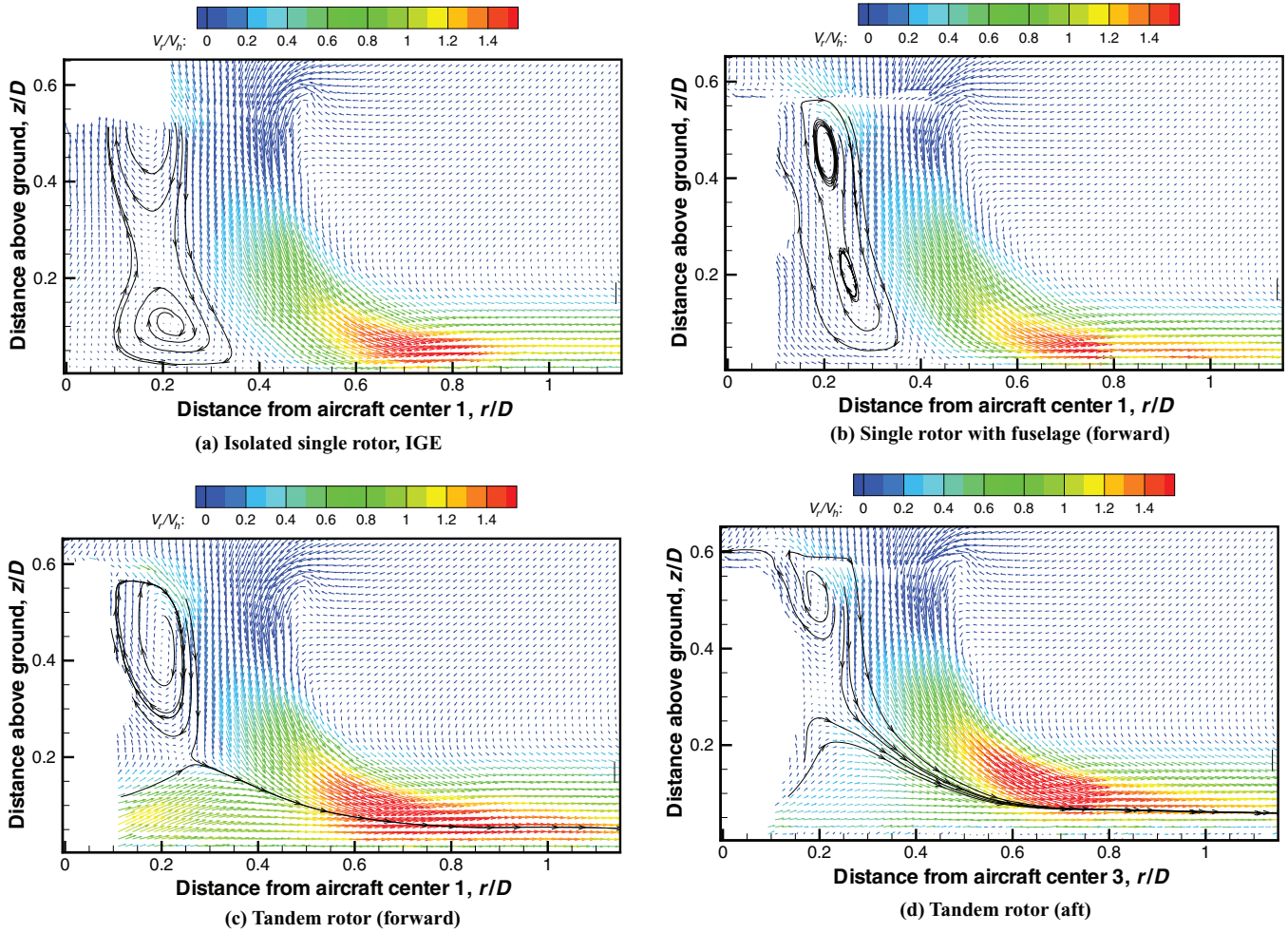


Fig. 8. Flow field comparison at $h/D = 0.578$ (see Fig. 2 for aircraft reference centers).

multiple regions for this study. Per the labels in Fig. 7, these include the contraction (Region 1), the transition (Region 2) where the flow changes from predominantly vertical to horizontal direction, and outwash (Region 3). Region 4 of the image corresponds to the recirculation zone ($V_r < 0$, flow direction toward the rotor), and is not analyzed in this study.

For each region, the following topics are explored: (1) IGE versus OGE for isolated single rotors, (2) effects of the fuselage for rotor IGE, (3) single versus multirotors (or the effects of aft rotor on the front rotor and vice versa) IGE, (4) differences in the rotorwash between the longitudinal and lateral axis of the tandem rotor IGE, and (5) effects of rotor height on rotorwash, IGE.

Region 1: Contraction. The contraction region corresponds to the area between the rotor plane and the vertical location where maximum wake contraction occurs. The time-averaged downwash velocities for the isolated single rotor, the single rotor with fuselage, and the tandem rotor system are shown in Fig. 8. All cases correspond to a rotor height (h/D) of 0.578. In the case of the tandem rotor system, velocities from both the forward and aft rotors are shown. Streamtraces are drawn to highlight important features present in the flow field.

In Fig. 7, the location of maximum wake contraction distinguishes Region 1 from 2. The absence of a defined border such as a tip vortex trajectory makes the distinction between Region 1 and 2 somewhat subjective. However, if the maximum downwash velocity defines the location of maximum wake contraction, Ref. 3 showed that Region 1

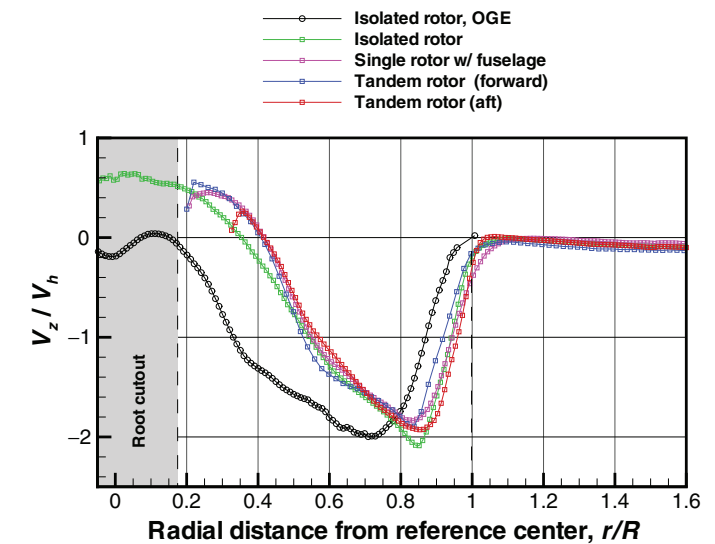


Fig. 9. Downwash velocity comparison below the rotor (at $z/D = 0.44$) for various rotor configurations.

extends to $0.17D$ beneath the rotor plane (i.e., $z/D \approx 0.44$) for all rotor configurations used in the present study.

Figure 9 shows the downwash velocity at $z/D = 0.44$ across the rotor disk for various rotor configurations. The changes to the inflow

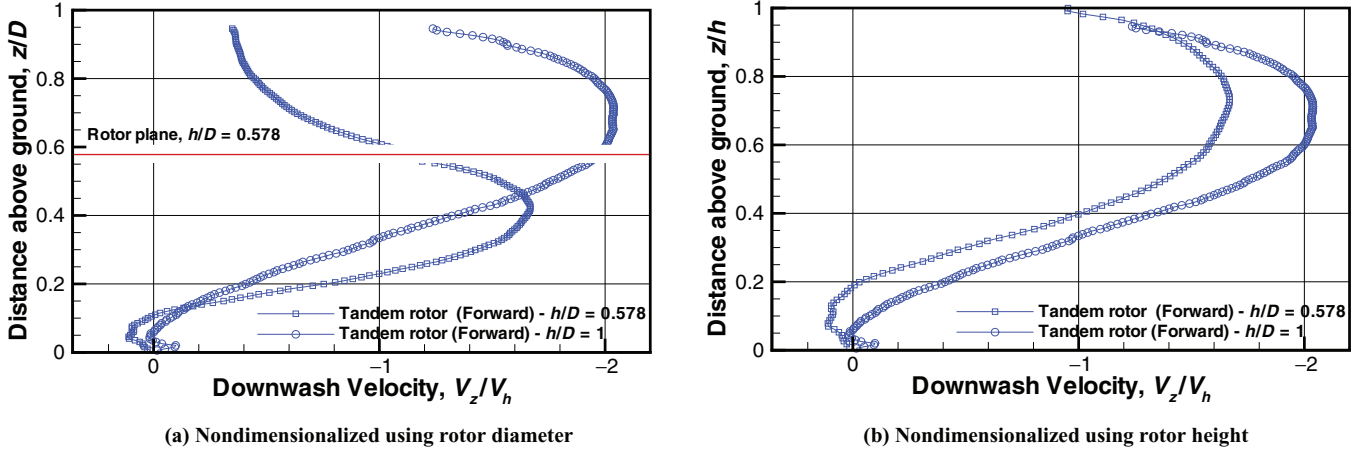


Fig. 10. Vertical velocity variation for two different rotor heights.

distribution are compared against the isolated single rotor operating OGE. The thrust conditions are such that $C_{T\text{ iso}} = C_{T\text{ forward}} = C_{T\text{ aft}} = 0.00305$, i.e., single-rotor thrust (OGE/IGE/with or without fuselage) is half the total system thrust of the model-scale tandem rotor. All rotor configurations operating IGE produced less downwash velocity than the isolated rotor operating OGE (inside the wake boundary defined as the change in V_z slope near $r/R = 0.8$).

Recirculation found near the blade root gained strength IGE, resulting in higher upwash velocities at the center of the rotor flow. For the isolated rotor IGE, the presence of the ground also appeared to have pushed the edge of recirculation radially outward from the shaft axis (identified by the higher r/R where V_z becomes positive). Comparing downwash velocities with and without fuselage, the fuselage pushed the region of recirculation even further outward with slightly higher upwash velocities. The maximum downwash velocity occurs over a small region for any rotor configuration operating IGE and is about $2 \times V_h$. This suggests that the average downwash beneath the rotor will be substantially lower than what is expected based on momentum theory (with uniform inflow assumption).

Figure 10(a) shows the tandem rotor system downwash velocity in front of the forward rotor. The measurement point corresponds to a vertical line at 75% blade span for two different rotor heights ($h/D = 0.578$ and 1.0). Increasing the hovering height of the rotor appears to increase the peak downwash velocity. In addition, the maximum wake contraction occurs near 30%D below the rotor versus 17%D at the lower height. However, when normalized with the rotor height above the ground (see Fig. 10(b)), the location of maximum downwash velocity is approximately 30% of rotor height ($z/h = 0.7$) below the rotor plane for both cases.

Vertical velocity profiles extracted from horizontal line cuts through the forward rotor flow field are shown for two different rotor heights in Fig. 11. For the case of $h/D = 1$, horizontal line cuts were made at two locations beneath the rotor, $z/D = 0.44$ and 0.66 , corresponding to the location of maximum downwash velocity for $h/D = 0.578$ and 1.0 , respectively. When comparing the velocity profiles at the same z/D , increasing rotor height appears to increase the downwash velocity across the entire rotor disk. This observation is expected based on the velocity profiles shown in Fig. 10(a). Also, comparing the two velocity profiles at the same rotor height ($h/D = 1$), the peak downwash velocity does not increase substantially with increasing distance below the rotor. Rather, consistent with the OGE behavior, momentum simply transfers from outboard to inboard where the low-momentum recirculation region exists.

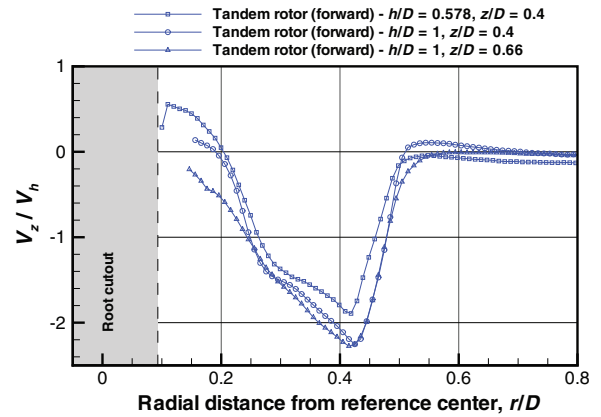


Fig. 11. Downwash velocity variation at two different rotor heights (using reference center 1 in Fig. 2).

Tandem rotor lateral axis. Velocity measurements made along the 90° and 270° azimuth stations (starboard and port, respectively) are shown in Fig. 12 for a rotor height of $h/D = 0.578$. The tandem configuration uses the reference center “2” identified in Fig. 2. The velocity contours represent the horizontal component of velocity. A key difference between the longitudinal and lateral axis is the absence of the recirculation zone below the rotor in the lateral axis. This is, however, expected because the inflow was provided only by the outboard sections of the blade (no rotor cut out) that produce positive lift.

Regarding the lateral axis, the flow along the starboard side (90° aircraft azimuth) emerges from the overlapping rotors by moving downward before gradually changing its direction away from the aircraft (Fig. 12(a)). In contrast, the port side showed nearly vertical flow over the entire overlap region (up to $r/D = 0.378$ where blade tips meet) for nearly the entire distance below the rotor up until very close to the ground (Fig. 12(b)). The observed difference in the flow pattern can be explained using the rotational direction of the two rotors, which is counterclockwise for the forward rotor and clockwise for the aft rotor. Because the rotors are spinning in opposite direction, the swirl resulting from the combined rotation aids radial outflow away from the aircraft on the starboard side while opposing the outflow on the port side.

Region 2: Transition region. The transition region exists between the location of maximum wake contraction below the rotor plane and the

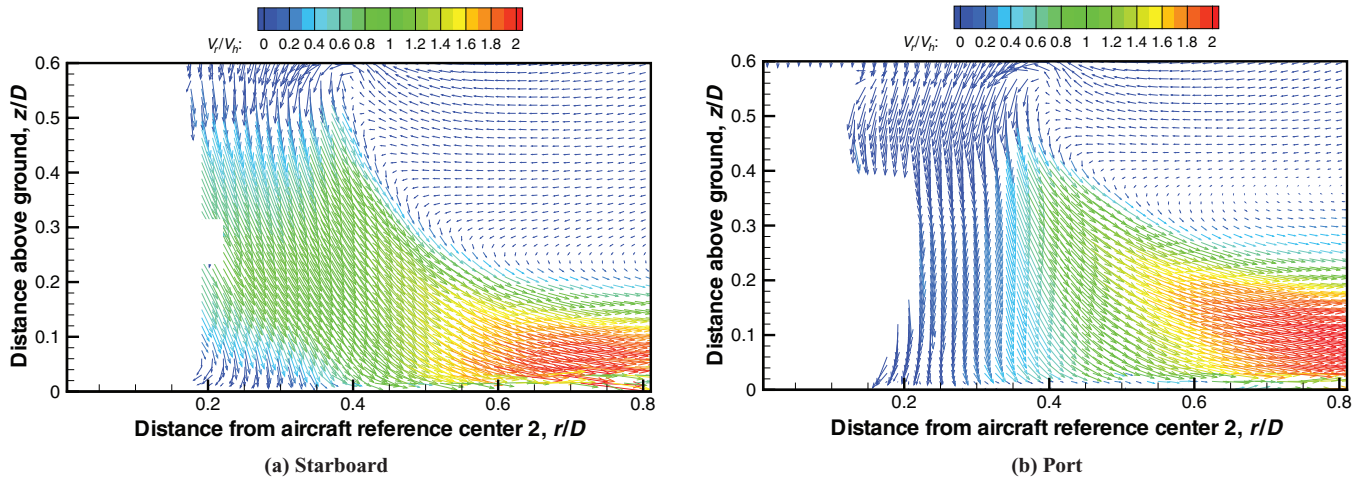


Fig. 12. Flow field comparison between starboard and port sides of the tandem rotor IGE at $h/D = 0.578$.

ground. Radially, the transition region covers the area between the shaft axis (or aircraft center in the case of the lateral planes) and the beginning of Region 3, where the wall jet starts. To analyze this region effectively, the horizontal velocity component (V_r) is plotted against normal distance (z/D) from the ground for all rotor configurations at several radial stations in Fig. 13. Velocity fields in Fig. 8 are used to augment Fig. 13 to understand the nature of flow in the transition region.

As mentioned earlier, Region 2 is a key area for personnel safety considerations and brownout initiation. For operations within the rotor outwash, an anthropometric model known as PAXman (Ref. 2) is used to compute forces on any approaching personnel. The red dotted line in Fig. 13 represents the height (5 ft 6 inches) of a 6-ft PAXman crouched and leaning while immersed in outwash.

In the cases of isolated single rotors, both with and without fuselage, Figs. 8(a) and 8(b) show that the recirculation region extends to the ground. The presence of the recirculation region results in a stagnation point on the ground. For the isolated rotor IGE (Fig. 8(a)), the stagnation point is located approximately $0.38D$ radially away from the shaft axis, meaning that any flow inside this point moves along the ground toward the rotor shaft ($r/D = 0$). Beyond the stagnation point, the flow moves radially away from the rotor. For the single rotor with fuselage (Fig. 8(b)), the stagnation point occurs at $42\%D$ from the shaft axis. The higher strength vortex near the ground can be inferred from the streamtraces in Fig. 8(b) as well as by comparing the V_r velocity magnitude exhibited by the green and magenta curves shown in Fig. 13(a). The single rotor with fuselage shows larger negative V_r near the ground than the isolated rotor IGE.

A stagnation region beneath an isolated rotor IGE has been identified in previous studies. For example, measurements on a model-scale isolated single rotor (Ref. 5) and a full-scale CH-53E rotor (Ref. 10) showed stagnation locations at $r/D = 0.25$ and 0.2 , respectively. Tuft flow visualization made beneath a UH-60L helicopter rotor also showed similar characteristics with the stagnation location at about $r/D = 0.33$ from the shaft axis (Ref. 16). The stagnation point and surrounding region (with low momentum) has been suggested as a safe place for ground personnel.

The difference between single rotors and the overlapping rotors of a tandem rotor system in the transition region first appears through the spatial location of the stagnation point. In the case of tandem rotor systems, Fig. 8(c) shows that the stagnation location for the front rotor moves substantially above the ground ($0.2D$) toward the rotor plane due to the flow from the aft rotor. This means that there is no flow toward the rotor (near the ground) in front of the forward rotor or downstream of the aft rotor unlike the single-rotor results (Fig. 8(b)).

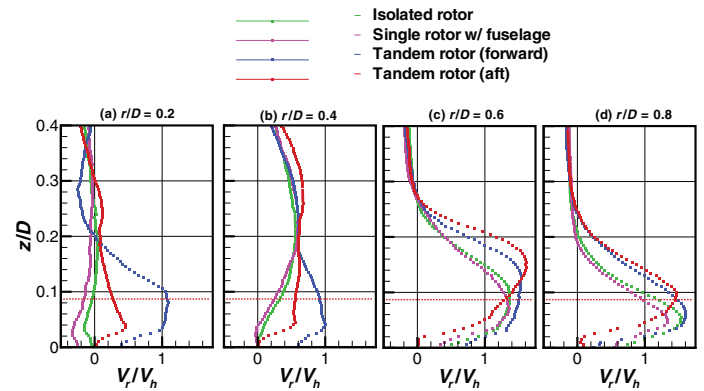


Fig. 13. Comparison of V_r velocity distribution normal to the ground in the transition region for all rotor configurations (PAXman height = $0.09D$).

Though a safe zone is absent beneath the rotors of the tandem rotor system, a relatively quiescent flow region may be present beneath the aircraft where a fountain-like flow may be expected (see Fig. 1(b)). However, no measurements were made beneath the aircraft to confirm this supposition. The magnitude and, more specifically, the direction of V_r found near the ground for the forward and aft tandem rotors (blue and red curves in Figs. 13(a) and 13(b)) may be important considerations for brownout. Also, because of the outflow from the aft rotor to the forward rotor (and vice versa) more fluctuations in the outwash along the longitudinal axis can be expected.

For the tandem rotor system, the flow exchange between forward and aft rotors strongly affects the radial velocity distribution. Figures 13(c) and 13(d) show the V_r distribution (outside the rotor disk) for two radial stations. Comparing the isolated rotor IGE and the single rotor with fuselage (IGE) with both operating at the same thrust, the isolated rotor seems to produce a stronger outwash. The peak measured V_r was 1.42 times the hover induced velocity from momentum theory, whereas that of the single rotor with fuselage was about 1.35. However, both the forward and aft rotors of the tandem rotor system (with each rotor operating at the same thrust as the single-rotor configuration) produced higher peak velocity (≈ 1.6) than all single-rotor configurations. In addition to the peak velocity magnitude, the normal distance from the ground where the peak occurs is also critical for human factors. Higher V_r velocity components away from the ground means that the overturning moments calculated on the PAXman will be higher.

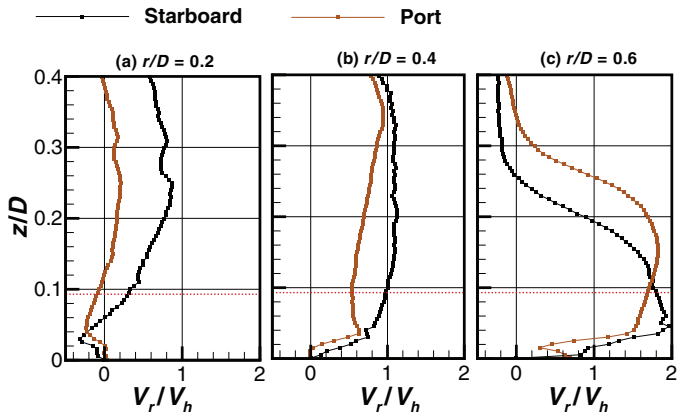


Fig. 14. V_r velocity distribution along the lateral axis of the tandem rotor system.

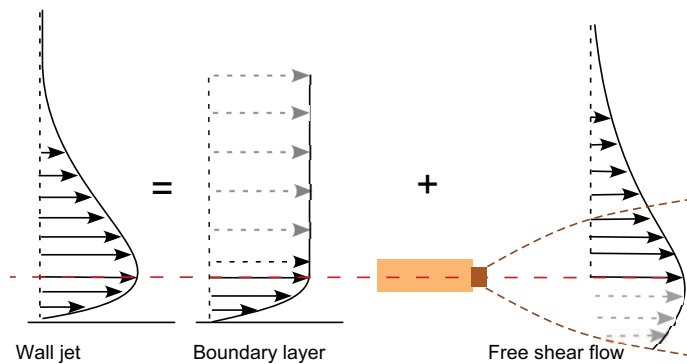


Fig. 15. Wall jet velocity profile as a combination of inner boundary layer and outer free jet.

At $r/D = 0.6$ (Fig. 13(c)), flow in front of the forward rotor has the highest V_r among the other configurations from the ground up to the height of the PAXman. Surprisingly, the aft rotor showed a more favorable V_r distribution at $r/D = 0.6$ even when compared against the single-rotor configurations. Above the height of PAXman, however, the aft rotor showed the highest velocity compared to the other rotors. Both tandem rotor system front and aft rotors showed fuller velocity profiles compared to the single rotors. At $r/D = 0.8$, observations similar to $r/D = 0.6$ can be made except for the expected reduction in velocity magnitudes.

Lateral axis. Figures 14(a)–14(c) show the V_r component of velocity at three radial stations, covering the transition region. Inside the rotor disk (i.e., $r/D < 0.5$), the horizontal component of velocity on the port side is always lower than the starboard over nearly the entire transition region below the rotor. Even outside the disk, i.e., at $r/D = 0.6$ and up to the height of PAXman, V_r is higher on the starboard side. However, slightly above the PAXman height (shown as a dotted red line), the port side shows the higher velocity. This trend is captured in full-scale measurements as well (Ref. 24). Though the effect of higher velocity above the PAXman may be less important from a personnel perspective, taller structures and ground equipment in the vicinity might be severely affected by the higher velocity. The maximum measured horizontal velocity was about twice the hover-induced velocity OGE, even though flow contribution comes from both rotors. Nevertheless, the observation was consistent with previous findings (Ref. 24) and such consistencies are essential for scalability studies.

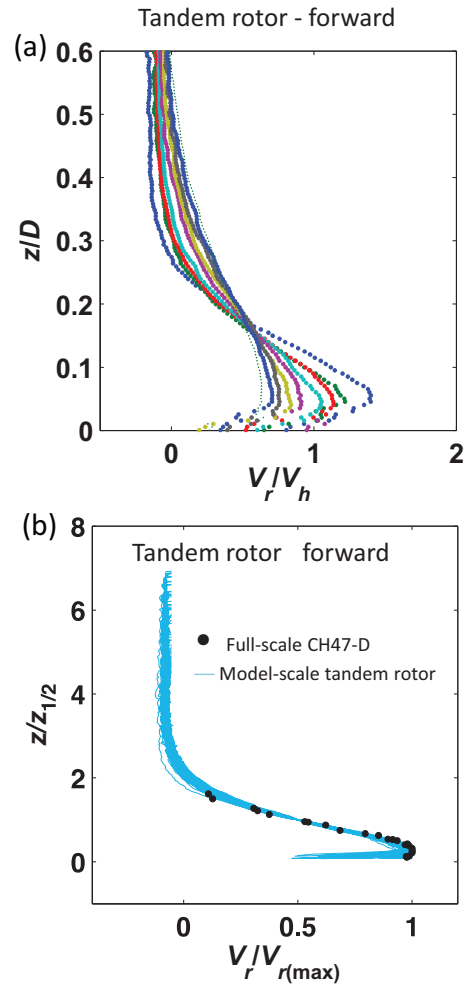


Fig. 16. Outwash velocity profiles at various radial distances nondimensionalized using (a) rotor coordinates and (b) wall jet-based similarity variables.

The flow along the lateral planes takes longer to resemble a wall jet because of the merging of inflow from two rotors. To simplify the analysis, parametric studies in this region are explored as part of the Region 3 discussion of outwash/wall jet analyses.

Region 3: Outwash. The research conducted on wall jets aids significantly in the rotor outwash analysis and scalability studies. Glauert coined the term “wall jet” to represent a jet flowing along the ground with quiescent flow above. Figure 15 shows the assumption made by Glauert, that is, the wall jet is a combination of two basic flows: a boundary layer in the inner layer and a free shear flow (jet from a nozzle) in the outer layer. Above the peak radial velocity, the flow behaves like a free shear flow. For a laminar radial wall jet (and for a turbulent radial wall jet with uniform eddy viscosity), Glauert derived a similarity solution proving that the wall jet profiles remain identical with radial distance provided that the flow parameters are nondimensionalized using peak radial velocity (at each radial station) and “ $z_{1/2}$.” The latter variable is the normal distance above ground where the velocity reaches half the peak value measured at the corresponding radial station. The outwash velocity decreases on either side of the peak value, resulting in two possible locations where the mean outwash velocity matches half the peak mean outwash velocity. Among the two choices, $z_{1/2}$ corresponds to the location above where peak velocity occurs. Other results of Glauert’s

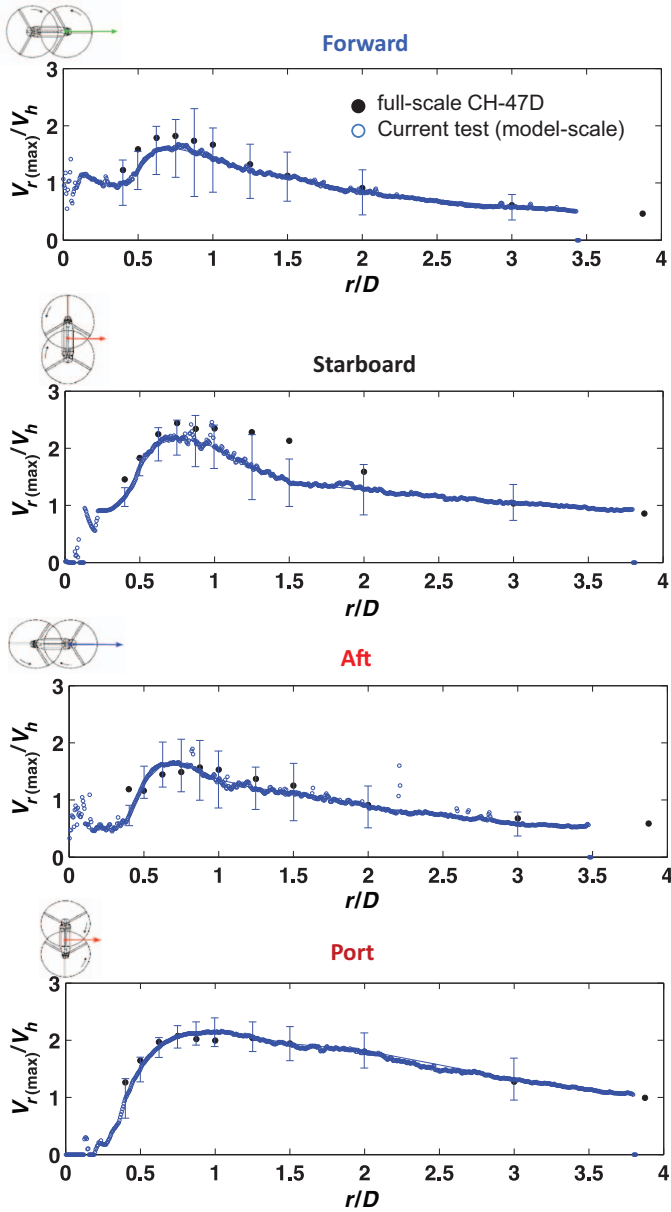


Fig. 17. Comparison of maximum radial velocity decay in the outwash region between model- and full-scale measurements.

analysis include estimation of the growth rate of the jet and the decay rate of the peak radial velocity with distance. George et al. (Ref. 30) applied the wall jet formulation to rotors for the first time when deriving the equivalent decay for outwash velocity.

Velocity profiles normalized using rotor parameters for radial distances greater than $r/D = 0.75$ are shown in Fig. 16(a). Using the wall jet parameters, $z_{1/2}$ and peak mean outwash velocity, normalized outwash profiles from $r/D = 0.75$ for the forward rotor (0° aircraft survey azimuth) are shown in Fig. 16(b). Because the velocities were normalized with the maximum measured outwash velocity, the entire analysis becomes independent of rotor parameters—allowing a direct comparison with full-scale measurements. Wall jet velocity profiles from multiple radial stations (vertical cuts made on the PIV measurement grid) coalesce into a single profile. Similar results were found for 90° , 180° , and 270° azimuths. Full-scale measurements, treated the same way, collapsed onto the model-scale data in Fig. 16, as expected. This result clearly suggests

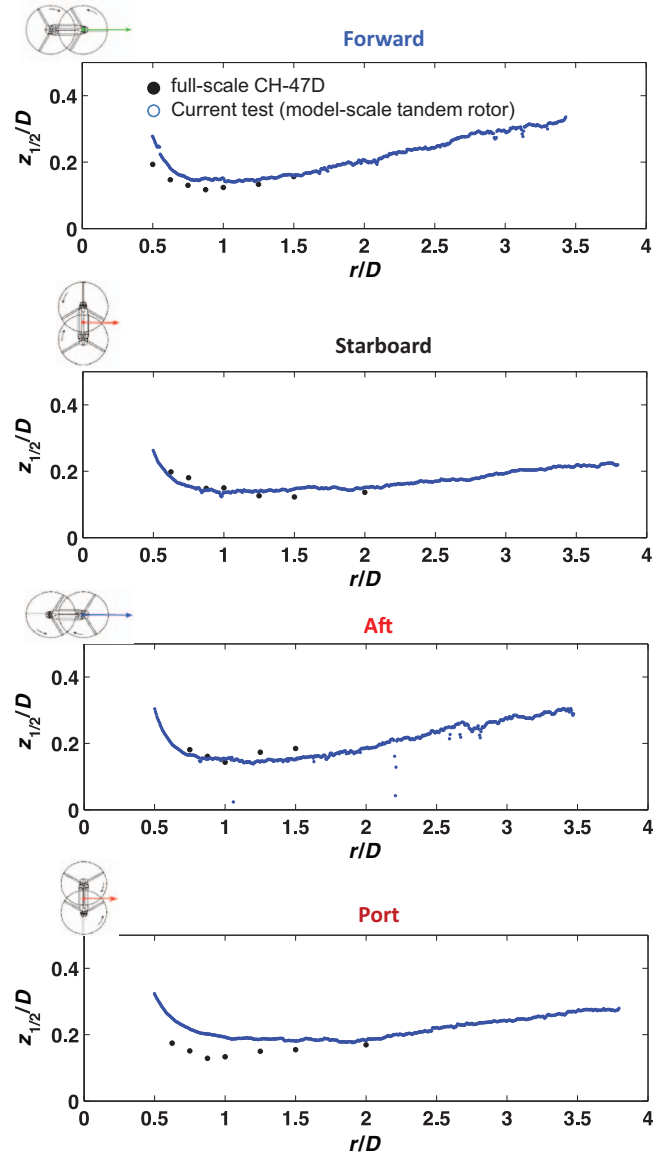
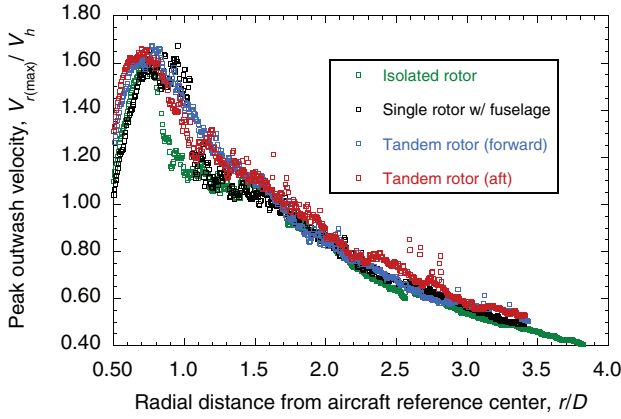


Fig. 18. Comparison of $z_{1/2}$ growth between model- and full-scale measurements.

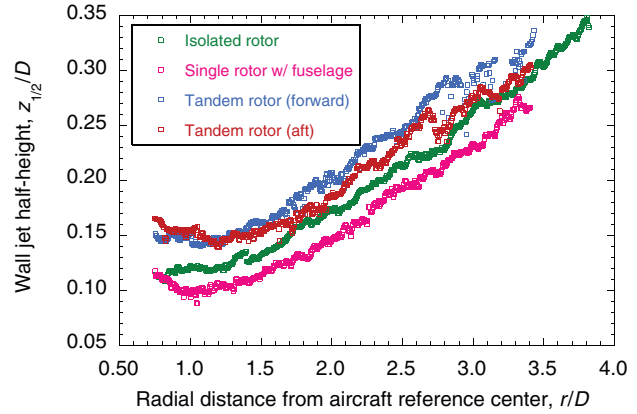
that model- and full-scale outwash velocity profiles are scalable in the front-aft and starboard-port planes using simple wall jet parameters, despite the interaction between the two rotors.

Matching wall jet outwash profiles between model- and full-scale alone does not guarantee that the model-scale replicates all the flow phenomena present in the full-scale rotor flow field. For example, velocity profiles would still match even if the turbulence levels are not scaled, i.e., velocity profiles may be self-similar and correlate well with full-scale data; however, the growth rate can be different. Only after comparing the decay of peak mean outwash velocity and the growth of $z_{1/2}$ between model- and full-scale (against radial distance) can scalability between model- and full-scale be confirmed.

Figure 17 shows the decay of peak mean outwash velocity with increasing radial distance on all four sides of the aircraft. Full-scale measurements are also plotted for comparison. The bars (σ) represent the model-scale velocity variation within the sampling time resulting from the periodic nature of the rotor flow. The bars are shown only at locations corresponding to full-scale measurement locations. Overall, the



(a) Peak mean outwash velocity decay



(b) Wall jet growth

Fig. 19. Peak mean outwash velocity decay and wall jet growth for various rotor configurations.

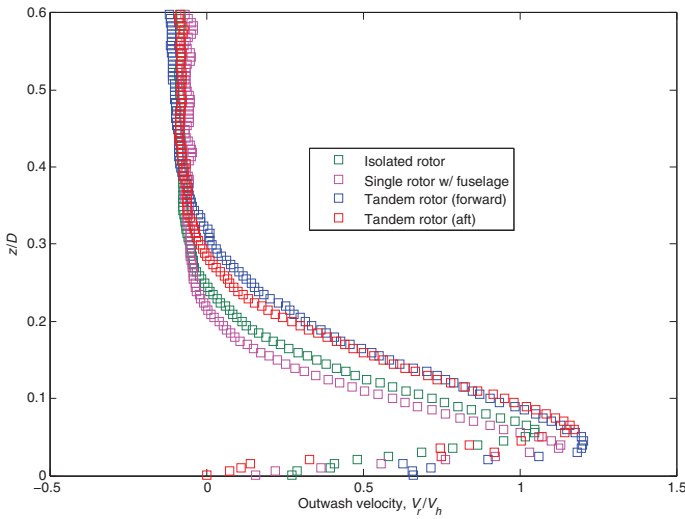


Fig. 20. Comparison of velocity profiles for various rotor configurations at $r/D = 1.25$ and $h/D = 0.578$.

correlation is good for all four directions at all radial distances, beginning from inside the rotor disk (transition region) to well outside ($r/D > 3.5$). Normalizing the radial distance with the diameter of the rotor appears to account for the scaling effects. Except for the 90° survey azimuth (starboard side) of the aircraft, especially for r/D between 1.25 and 2.0, all full-scale measurements lie within the periodic variations of model-scale measurements.

The outwash acceleration within the transition region, followed by decay in the wall jet region, is captured well. Comparing all four sides of the aircraft, the forward-aft plane produced lower peak outwash velocities ($V_{r(max)}/V_h \approx 1.6$) in the near wake ($r/D < 1.0$) than the starboard-port plane ($V_{r(max)}/V_h \approx 2.2$), as expected from the overlapping rotors. The starboard side produced the highest outwash velocity among the four sides of the aircraft.

The half-height of the wall jet profile ($z_{1/2}$) versus radial distance is plotted in Fig. 18 for all four sides of the aircraft. For both the forward and aft rotors, the $z_{1/2}$ growth began with the start of outwash velocity decay, i.e., $r/D > 0.75$. However, on the starboard and port sides, up until $r/D \approx 2.0$, no noticeable growth was found. The growth of $z_{1/2}$ began only after $r/D > 2$, and the growth rate was much slower compared to that in the forward and aft directions.

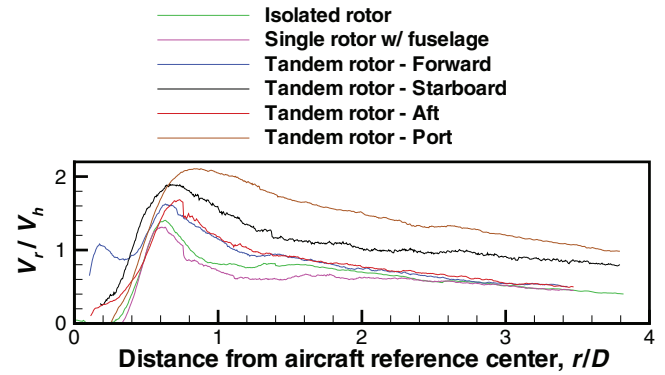


Fig. 21. V_r velocity at 5 ft 6 inches above the ground plane for all rotor configurations.

Using the three key parameters of wall jet analysis (outwash velocity profile, peak mean outwash velocity decay, and $z_{1/2}$ growth) and applying them to both model- and full-scale data, Figs. 16–18 clearly show the data from the model-scale tandem rotors replicate full-scale outwash data when normalized by appropriate rotor and flow variables. There is similarity between small- and full-scale outwash when the rotors interact lightly (i.e., forward-aft directions) or heavily (starboard-port directions). With these parameters, the outwash velocity profile at any radial location can be determined. The outwash velocity profiles normalized with V_h and rotor diameter (D) at several radial stations around the aircraft are reported in Ref. 3 along with full-scale measurements for reference.

Having established the similarity of model-scale rotor outwash to full-scale, parametric studies were conducted to provide further understanding of the interaction between the rotors, fuselage, and ground.

Parametric studies

Figures 19 and 20 show the velocity decay, $z_{1/2}$ growth, and the outwash velocity profile for all rotor configurations (isolated rotor IGE, single rotor with fuselage, and tandem rotor system (forward and aft rotors)). In the wall jet region (i.e., $r/D > 0.75$), maximum outwash measured for all rotor configurations are of the same order. However, the wall jet half-height is different for each configuration. Both the front and aft rotors of the tandem rotor system showed higher $z_{1/2}$ than the single rotors (both with and without fuselage).

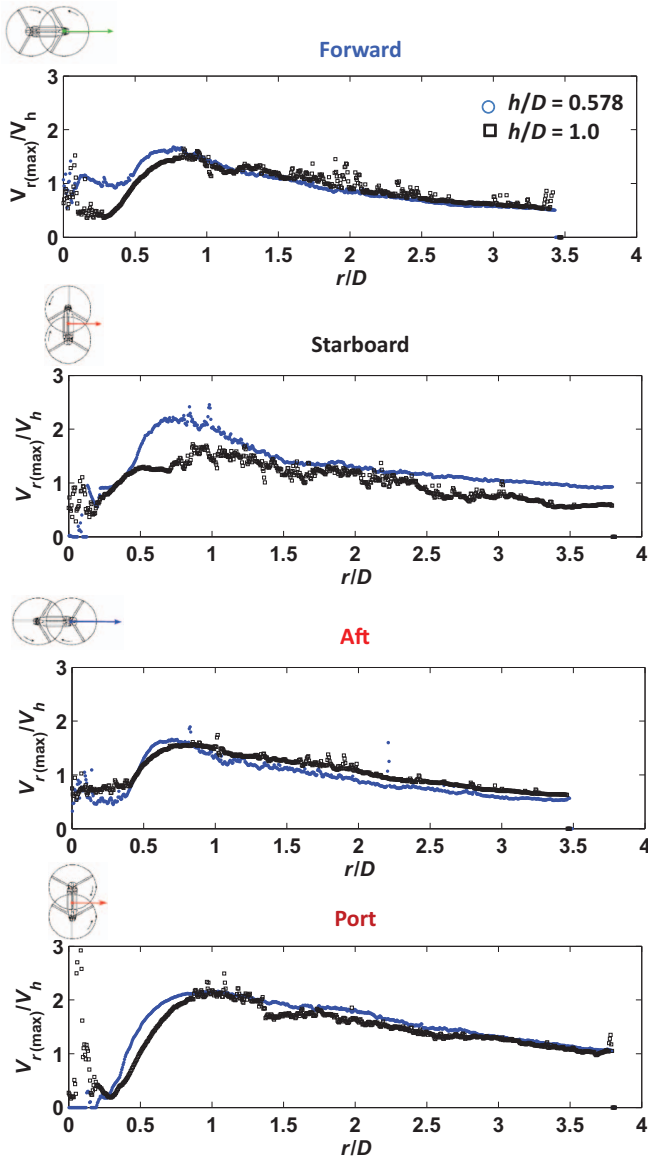


Fig. 22. Comparison of maximum velocity decay in the wall jet region for two different rotor heights.

The peak mean outwash velocity from a PAXman perspective is provided in Fig. 21 for all four configurations, which shows the radial outwash distribution for a rotor h/D of 0.578. This is a representative height equivalent to the full-scale PAXman height (5 ft 6 inches) of $z/D \approx 0.09$. The forward and aft rotors of the tandem rotor system produced higher outwash than the single rotors (with or without fuselage) near the rotor. As the radial distance increases, they all coalesce into a single curve suggesting tandem rotor systems have higher rate of decay at least in the near wake. For the tandem rotor configuration, up until $r/D = 0.65$, the starboard side of the rotor produced maximum outwash velocity. However, as radial distance increased, the port side produced the highest velocity. Again, these characteristics of maximum outwash velocity relative to all four sides are consistent with full-scale measurements at a ground height of 5 ft reported in Ref. 24. This observation is unexpected based on the direction of rotation of the two rotors and the expected higher velocity on the starboard side resulting from the favorable swirling effects of the two rotors. Furthermore, the outwash velocities along the

$90^\circ-270^\circ$ plane of the tandem rotor system remains high (with low decay) even at large radial distances compared with the $0^\circ-180^\circ$ plane.

Figure 22 shows the outwash velocity decay on all four sides of the aircraft for two different rotor heights above the ground plane. Several interesting observations were made. For the forward and aft directions, the maximum velocity decreased with increasing rotor height close to the rotor ($r/D < 0.7$). However, as the radial distance increased, the measured peak velocity was higher when the rotor height was increased. A PAXman standing at two different distances from the descending aircraft will feel different flow behavior. A PAXman standing closer to the rotor landing location will experience higher and higher velocity as the aircraft approaches the ground. However, a PAXman standing farther away will experience reduced velocities with decreasing rotor height. In the literature, the effects of rotor height on peak mean outwash velocity has been a contradictory issue (Refs. 9,13). However, those discrepancies arise mainly because of the differences in the measurement locations relative to the aircraft.

The similarities and differences found between $0^\circ-180^\circ$ and $90^\circ-270^\circ$ planes discussed above are also observed in the full-scale CH-47D measurements (Ref. 24), further validating the similarity of model-scale outwash to represent a full-scale outwash flow field.

While the observations made in the $0^\circ-180^\circ$ plane, in terms of radial variation of outwash velocity magnitude versus rotor height, are consistent with wall jet behavior, the observations made in the $90^\circ-270^\circ$ plane are not. Therefore, to predict outwash behavior for different rotor heights above the ground, a jet formulation should be reevaluated along the $90^\circ-270^\circ$ plane of a tandem rotor configuration.

Conclusions

A series of experiments was conducted to identify and understand various flow phenomena contributing to tandem rotor downwash and outwash. To simplify the problem, flow field measurements were carried out on a single isolated rotor IGE, followed by single rotor with fuselage, and then a complete tandem rotor system model with overlapping rotors. A single isolated rotor OGE served as the baseline configuration.

Scalability studies were conducted by comparing the present model-scale measurements with full-scale measurements in terms of observations, trends, and flow variables such as downwash and outwash velocities after normalizing with rotor and/or wall jet variables. Specific conclusions derived from the present study are enumerated below.

Configuration effects

1) A stagnation location that would facilitate ground personnel operation beneath a single hovering rotor was found at $r/D = 0.38$ and 0.42 for an isolated rotor and single rotor with fuselage, respectively. A stagnation location at the ground was not found beneath the tandem rotor system.

2) In the wake contraction and transition region, the vertical component of velocity was of the same order for both starboard and port side for the tandem rotor system. However, the horizontal component was much higher on the starboard side than the port side—a consequence of the direction of rotation of the two rotors relative to the fuselage and the resulting swirling flow.

3) The horizontal component of velocity for the tandem rotor (forward and aft rotor) was higher in the transition region than for single rotors (with or without fuselage) due to flow interaction between the forward and aft rotor. Modeling the flow in front of the forward rotor (or downstream of the aft rotor) must include the flow contribution from the other rotor in the near wake. As radial distance increased, however,

the normalized outwash velocities from all configurations (tandem and single) collapsed to a single curve.

4) Fore/Aft outwash velocity profiles were fuller for the tandem rotor system compared with single rotors with or without fuselage.

5) Peak mean outwash velocity decay began at $r/D = 0.75$ for single rotors (with and without fuselage) and for the tandem rotor system front and aft rotors. The growth of the wall jet width ($z_{1/2}$) also began near $r/D = 0.75$ for these configurations. However, along the 90° – 270° plane, wall jet characteristics ($z_{1/2}$ growth) of the tandem rotor system began near $r/D > 2.0$.

Scalability studies

1) All three characteristics of the wall jet, i.e., outwash velocity profile, peak mean outwash velocity, and $z_{1/2}$ growth on all four sides of the model-scale tandem rotor system correlated well with full-scale measurements.

2) Increased rotor height above the ground increased maximum downwash velocity measured below the rotor (at maximum contraction). The location where maximum wake contraction occurred below the rotor, when normalized with rotor height, remained at $30\%(h/D)$.

3) Increasing rotor height above the ground decreases the outwash velocity near the rotor for all four sides of the aircraft. However, for $r/D > 1$, the peak mean outwash velocity increased with increasing rotor height for the aircraft longitudinal axis. Along the lateral axis, outwash velocity decreased at all radial distances for increased rotor height. The data from the full-scale CH-47D exhibited similar behavior. Although a wall jet analogy is appropriate for the longitudinal plane, the same analogy cannot be applied to the flow in the lateral plane.

4) The peak mean outwash velocity was found to be the highest along the 90° (starboard) aircraft survey azimuth near the rotor compared to the other three sides of the aircraft. However, farther out from the rotor, the 270° aircraft survey azimuth (port side) showed higher outwash velocity than 90° . These characteristics are consistent with full-scale CH-47D data.

Acknowledgments

The authors gratefully acknowledge Mr. Mark Silva for his helpful discussions of the full-scale CH-47D outwash measurements. The authors also acknowledge Drs. John Preston and Samuel Ferguson for providing rare experimental/analysis reports of previous work, and for numerous discussions on the development of the RoWFoot model. The support of Mr. Perry Kavros in setting up the experiment and keeping the rotor operational through several months of rigorous testing is greatly appreciated.

References

¹Schane, L.T.C. W. P., "Effects of Downwash Upon Man," U.S. Army Aeromedical Research Unit, Fort Rucker, AL, Report No. 68-3, November 1967.

²Preston, J. R., Troutman, S., Keen, E., Silva, M., Whitman, N., Calvert, M., Cardamone, M., Moulton, M., and Ferguson, S. W., "Rotorwash Operational Footprint Modeling," U.S. Army RDECOM Technical Report RDMR-AF-14-02, July 2014

³Ramasamy, M., Potsdam, M. S., and Yamauchi, G. Y., "Measurements to Understand the Flow Mechanisms Contributing to Tandem-Rotor Outwash," American Helicopter Society 71st Annual Forum Proceedings, Virginia Beach, VA, May 5–7, 2015.

⁴Taylor, M. K., "A Balsa-Dust Technique for Air-Flow Visualization and Its Application to Flow through Model Helicopter Rotors in Static Thrust," NACA TN 2220, November 1950.

⁵Fradenburgh, E. A., "Flow Field Measurements for a Hovering Rotor Near the Ground," American Helicopter Society Fifth Annual Western Forum Proceedings, Los Angeles, CA, September 25–26, 1958.

⁶Bolanovich, M., and Marks, M. D., "Experimental Downwash Velocity, Static Pressure, and Temperature Distributions in Ground Effect for a 75-ft Jet Driven Rotor," *Journal of the American Helicopter Society*, Vol. 4, (2), April 1959, pp. 22–36.

⁷Bryan, T. O. "Considerations of the Effect of VTOL Downwash on the Ground Environment," NASA Conference on V/STOL Aircraft, Hampton, VA, November 17–18, 1960, pp. 261–268.

⁸Newsom, W. A., and Totsi, L. P., "Slipstream Flow around Several Tilt-Wing VTOL Aircraft Models Operating Near Ground," NASA TN D-1382, September 1962.

⁹Michaelsen, O. E., "A Comparison of Outflows from a Helicopter, Tilt Wing and Jet Lift Hovering Aircraft," AIAA 71-992, AIAA 8th Annual Meeting and Technology Display, Washington, DC, October 25–28, 1971.

¹⁰Harris, D. J., and Simpson, R. D., "Downwash Evaluation under the U.S. Army Heavy Lift Helicopter Rotor: Final Report," Naval Air Test Center Technical Report No. SY-17R-76, March 16, 1976.

¹¹Velkoff, H., and Sheppard, A., "The Utilization of Helicopter Technology in the Prevention of Frost in Orange Groves," 11th European Rotorcraft Forum, London, UK, September 10–13, 1985.

¹²Light, J. S., "Tip Vortex Geometry of a Hovering Helicopter Rotor in Ground Effect," American Helicopter Society 45th Annual Forum Proceedings, Boston, MA, May 22–24, 1989.

¹³Meyerhoff, C., "Navy Developmental Test (DT-IIA) of the MV-22 Aircraft Contributory Test Report: Rotor Downwash," Naval Air Test Center Technical Report ACS-CR-90-04, SY71A, Summer 1990.

¹⁴Lake, R. E., and Clark, W. J., "V-22 Rotor Downwash Survey," NAWCADPAX-98-88-RTR, July 1998.

¹⁵Wadcock, A. J., "Rotor Outwash," Unpublished Presentation Made to U.S. Army, October 2005.

¹⁶Wadcock, A. J., Ewing, L. A., Solis, E., Potsdam, M., and Rajagopalan, G., "Rotorcraft Downwash Flow Field Study to Understand the Aerodynamics of Helicopter Brownout," American Helicopter Society Southwest Region Technical Specialists Meeting, Dallas-Fort Worth, TX, October 15–17, 2008.

¹⁷Nathan, N. D., and Green, R. B., "Measurements of a Rotor Flow in Ground Effect and Visualization of the Brown-out Phenomenon," American Helicopter Society 67th Annual Forum Proceedings, Montreal, Canada, April 29–May 1, 2008.

¹⁸Johnson, B. S., Leishman, J. G., and Sydney, A., "Investigation of Sediment Entrainment Using Dual-Phase, High-Speed Particle Image Velocimetry," *Journal of the American Helicopter Society*, **55**, 042003 (2010).

¹⁹Lee, T. E., Leishman, J. G., and Ramasamy, M., "Fluid Dynamics of Interacting Blade Tip Vortices with a Ground Plane," *Journal of the American Helicopter Society*, **55**, 022005 (2010).

²⁰Wong, O. D., and Tanner, P. E., "Photogrammetric Measurements of an EH-60L Brownout Cloud," *Journal of the American Helicopter Society*, **61**, 012003 (2016).

²¹Milluzzo, J., Sydney, A. B., Rauleder, J., and Leishman, J. G., "In-Ground-Effect Aerodynamics of Rotors with Different Blade Tips," American Helicopter Society 66th Annual Forum Proceedings, Phoenix, AZ, May 11–13, 2010.

²²Milluzzo, J., and Leishman, J. G., "Assessment of Rotorcraft Brownout Severity in Terms of Rotor Design Parameters," *Journal of the American Helicopter Society*, **55**, 032009 (2010).

²³Sydney, A. B., and Leishman, J. G., "Understanding Brownout Using Near-Wall Dual-Phase Flow Measurements," American Helicopter

Society 67th Annual Forum Proceedings, Virginia Beach, VA, May 3–5, 2011.

²⁴Silva, M. J., and Riser, R., “CH-47D Tandem Rotor Outwash Survey,” American Helicopter Society 67th Annual Forum Proceedings, Virginia Beach, VA, May 3–5, 2011.

²⁵Glaser, M. S., and Jones, A. R., “Effects of Model Scaling on Sediment Transport in Brownout,” 30th AIAA Applied Aerodynamics Conference, New Orleans, LA, June 25–28, 2012.

²⁶George, M., Perlmutter, A. A., and Butler, L., “Downwash Impingement Criteria for VTOL Aircraft,” TRECOM Technical Report 64-48, U.S. Army Aviation Material Laboratories, Fort Eustis, VA, July 1964.

²⁷Glauert, M. B., “The Wall Jet,” *Journal of Fluid Mechanics*, Vol. 1, (6), December 1956, pp. 625–643.

²⁸Derby, M. D., and Yamauchi, G. K., “Design of 1/48th-Scale Models for Ship/Rotorcraft Interaction Studies,” AIAA 2003-3952, 21st Applied Aerodynamics Conference, Orlando, FL, June 23–26, 2003.

²⁹Spalart, P. R., “On the Flow Field Induced by a Hovering Rotor or a Static Jet,” *Journal of Fluid Mechanics*, Vol. 701, May 2012, pp. 473–481.

³⁰George, M., Kisielowski, E., and Douglas, D. S., “Investigation of the Downwash Environment Generated by V/STOL Aircraft Operating in Ground Effect,” USAAVLABS Technical Report 68-52, July 1968.